Journal of Applied Polymer Science

Structural and antibacterial properties of a γ-radiation-assisted, *in situ* prepared silver–polycarbonate matrix

A. V. Deore,[1] K. Hareesh,[1] P. Ramya,[2] E. Ianni,[2] P. Guagliardo,[3] S. Samarin,[2] J. F. Williams,[2] G. Sanjeev,[4] S. S. Dahiwale,[1] D. Kanjilal,[5] N. A. Dhole,[6] K. M. Kodam,[6] V. N. Bhoraskar,[1] S. D. Dhole[1]

[1]Microtron Accelerator Laboratory, Department of Physics, Savitribai Phule Pune University, Pune 411007, India
[2]ARC Centre for Antimatter–Matter Studies, School of Physics, University of Western Australia, Crawley, Western Australia 6009, Australia
[3]Centre for Microscopy, Characterisation, and Analysis, University of Western Australia, Crawley, Western Australia 6009, Australia
[4]Microtron Centre, Department of Studies in Physics, Mangalore University, Mangalore 574199, India
[5]Inter-University Accelerator Centre, New Delhi 110067, India
[6]Department of Chemistry, Savitribai Phule Pune University, Pune 411007, India
A. V. Deore and K. Hareesh contributed equally to this article.
Correspondence to: K. Hareesh (E-mail: appi.2907@gmail.com) and S. D. Dhole (E-mail: sanjay@physics.unipune.ac.in)

ABSTRACT: A silver–polycarbonate (Ag–PC) matrix was prepared by a γ-radiation-assisted diffusion method, and its antibacterial properties were studied. Rutherford backscattering spectroscopy, X-ray diffraction, and transmission electron microscopy results showed the diffusion of good, crystalline-structured (face-centered cubic) silver nanoparticles (AgNPs) inside polycarbonate (PC) after irradiation. Ultraviolet–visible spectroscopic results indicated a blueshift in the surface plasmon resonance of the AgNPs; this revealed a particle size decrease with increasing γ-radiation dose. This was also supported by the scanning electron microscopy results. The microstructure of the pristine PC and silver-doped PC was monitored with positron annihilation spectroscopy, and it showed decreases in the free-volume hole size and fractional free-volume for Ag–PC and γ-ray-irradiated PC. This corroborated the Doppler broadening spectroscopy results. The thermal degradation temperature of PC was increased because of the diffusion of AgNPs in PC. The antibacterial activity of the synthesized Ag–PC matrix was evaluated by the zone of inhibition, and the results demonstrated its bacterial growth inhibition ability. The results indicate the potential to produce an Ag–PC matrix for various applications in medical and food industries. © 2016 Wiley Periodicals, Inc. J. Appl. Polym. Sci. **2016**, *133*, 43729.

KEYWORDS: irradiation; nanostructured polymers; polycarbonates

Received 26 October 2015; accepted 1 April 2016
DOI: 10.1002/app.43729

INTRODUCTION

The synthesis of noble metal nanoparticles have been investigated extensively because of their optical, catalytic, and electronic properties. Among various noble metal nanoparticles, silver nanoparticles (AgNPs) have attracted much attention because of their applications in several fields, including optoelectronics, information storage, biomedical imaging, catalysis, and antibacterial applications.[1] Several methods have been reported for the synthesis of AgNPs; these include chemical reduction, photoreduction, an electrochemical method, atom beam sputtering, and a radiation-assisted method.[2] Among all these, the radiation-assisted, *in situ* synthesis of AgNPs has been termed a simple, clean, and efficient method.[3]

The synthesis of AgNPs in a polymer matrix by the irradiation method has gained much attention because of its advantages over other methods, as it is environmentally friendly and prevents the use of harsh reducing agents.[3] The synthesis of AgNPs 40–150 nm in size in poly(vinyl alcohol) by low-energy electrons was reported by Mahapatra *et al.*[4] Bogle *et al.*[5] synthesized AgNPs with sizes in the range 100–200 nm in poly(vinyl alcohol) by 6-MeV electron-beam irradiation. Pattabi *et al.*[6] studied the growth and stability of AgNPs in poly(vinyl alcohol) by 8-MeV electron-beam irradiation. A comparative study of γ-ray, electron-beam, and synchrotron X-ray irradiation methods for the synthesis of AgNPs in poly(vinyl pyrrolidone) was carried out by Misra *et al.*,[7] and they concluded that the particle size distribution was larger in case of γ-ray irradiation compared to

that of electron beams and synchrotron X-rays. Recently, Vacik *et al.*[8] studied the diffusion of silver (Ag) into polyimide, high-density polyethylene, and poly(ether ether ketone) by *in situ* electron irradiation. The ultraviolet-assisted *in situ* synthesis of AgNPs on silk fibers for antibacterial applications was reported by Lu *et al.*[9] γ-radiation was used by many researchers for the synthesis of AgNPs in poly(vinyl alcohol)[10–12] and in poly(vinyl pyrrolidone).[13–15] Mukherjee *et al.*[16] studied the annihilation characteristics of positrons in polyacrylamide containing AgNPs. Positron annihilation spectroscopy (PAS) of trimethylol propane trimethacrylate silica was reported by Zaleski *et al.*[17] The free-volume properties in a system of 20-nm zinc oxide nanoparticles dispersed in waterborne polyurethane were measured with positron annihilation lifetime spectroscopy by Awad *et al.*[18] However, there is a lacuna in the literature for the PAS study of silver–polycarbonate (Ag–PC). γ irradiation alters the microstructural properties of polymers through several routes, for example, chain scission/crosslinking, the creation of free radicals, and changes in the fractional free volume (F_V).[19–21] Information about chain scission/crosslinking and changes in F_V can be accurately obtained by the PAS technique because of its efficacy in the detection of free-volume holes at the subatomic level and its high sensitivity for microstructural changes. In polymers, *ortho*-positronium (*o*-Ps; metastable bound state of electrons and positrons with parallel spin) preferentially localizes and annihilates in the free-volume holes of a polymer.[22] This characteristic of *o*-Ps makes it the microprobe of choice, and its lifetime and intensity become a measure of the electron density and free-volume size in the study of the microstructural behavior of polymers.[22–25]

This article deals with the synthesis of an Ag–PC matrix by a γ-radiation-assisted, *in situ* method and their characterization by Rutherford backscattering spectroscopy (RBS), ultraviolet–visible (UV–vis) spectroscopy, X-ray diffraction (XRD), scanning electron microscopy (SEM) attached with energy-dispersive spectroscopy (EDS), transmission electron microscopy (TEM), thermogravimetric analysis (TGA), Fourier transform infrared (FTIR) spectroscopy, and its free-volume study by PAS and Doppler broadening (DB) spectroscopy measurements. The antibacterial properties of the prepared samples were also checked by an agar diffusion method against a Gram-negative bacteria (*Escherichia coli*) and Gram-positive bacteria (*Staphylococcus aureus*). These two bacteria spread via water or meat and may cause serious food poisoning, anemia, fever, and more. Therefore, it is important to synthesize a nanoparticle-diffused polymer matrix that will inhibit these kinds of bacteria. In this study, we prepared an Ag–PC matrix by a γ-radiation-assisted method and studied it effectively for the inhibition of the overall growth of these types of bacteria.

MECHANISM OF FORMATION AND DIFFUSION OF AgNPs

The process of metal nanoparticle synthesis by radiolysis can be depicted by the following reactions:

$$n \cdot H_2O \xrightarrow{\gamma-\text{irradiation}} e_{aq}^-, H^{\cdot}, OH^{\cdot}, H_2, H_3O^+, H_2O_2, \ldots\ldots \text{etc} \quad (1)$$

$$e_{aq}^- + Ag^{n+} \rightarrow Ag^{(n-1)+} \quad (2)$$

$$e_{aq}^- + Ag^{n+} \rightarrow Ag^0 \quad (3)$$

In the radiolytic method, aqueous solution is exposed to high-energy γ-rays to generate free electrons through Compton scattering. During γ-ray exposure, they also produce species, such as hydrated electrons (e_{eq}^-) and hydrogen radicals arising from the radiolysis of water.[26] Ag ions will get reduced to a zero-valent state by the generated electrons, which are strong reducing agents. In turn, electrons reduce Ag ions into Ag atoms. These Ag atoms are transferred into the free volume in the polycarbonate (PC) created during γ irradiation by thermal activation. During irradiation, the rate of diffusion is governed by the net concentration of free volume in the polymer matrix. The neutral atoms transferred to the defect sites start coalescing to form aggregation of AgNPs in the polymer as depicted by following reaction. Simultaneously, the reduced Ag atoms start coalescing to form colloidal metal nanoparticles in the solution:[15]

$$nAg^0 \rightarrow (Ag)_2 \rightarrow \ldots (Ag)_n \ldots \rightarrow (Ag)_{agg} \quad (4)$$

The nanoparticles size is related to the γ-ray dose, and it is well explained in the report of Naghavi *et al.*[27] For Ag ions, the electron capture is high, and this produces a large number of neutral Ag atoms:

$$Ag^+ + e_{aq}^- \rightarrow Ag^0 \quad (5)$$

$$Ag^0 + Ag^0 \rightarrow Ag_2 \quad (6)$$

The bonding between neutral atoms/clusters with unreduced ions is also strong, and hence, association between them occurs quickly.[27] The neutral Ag atoms and unreduced Ag ions combine results in the formation of AgNPs:

$$Ag^0 + Ag^+ \rightarrow Ag_2^+ \quad (7)$$

$$Ag_m + Ag^+ \rightarrow Ag_{m+1}^+ \quad (8)$$

$$Ag_{m+1}^+ + e_{aq}^- \rightarrow Ag_{m+1} \quad (9)$$

The last two reactions [eqs. (8) and (9)] of ion association with atoms/clusters are fast and important in the cluster growth mechanism. There is the simultaneous reduction of free Ag ions and absorbed ones, and both are controlled by the rate of formation of reducing radicals. Cluster formation by direct reduction followed by coalescence is dominant at higher γ-ray doses, and the final aggregates are smaller in size compared to those formed at lower doses. In the case of higher doses, the adsorption of ions takes place on neutral Ag atoms or small clusters formed at an earlier stage. This process is independent and cannot be controlled by the reduction *in situ* of ions by electron transfer from reducing radicals. The electrons from smaller aggregates can be transferred to larger ones coated with adsorbed ions.[27] In this manner, during γ-ray irradiation, the number of AgNPs increases, and Ag particles of nanometric dimensions can be synthesized.

EXPERIMENTAL

Preparation of the Ag–PC Matrix

We prepared an $AgNO_3$ solution (1 m*M*) by dissolving $AgNO_3$ in double-distilled water and stirring it for 30 min. A volume of

10 mL of this solution was put into a glass bottle. PC ($C_{16}H_{14}O_3$; Lexan) with a size of $1.5 \times 1.5\,cm^2$ and a thickness of 200 μm was immersed in the glass bottle containing the $AgNO_3$ solution. This bottle was exposed to a Co-60 γ-radiation chamber (dose rate = 5.4 kGy/h), and a 50-kGy irradiation dose was delivered. A similar type of experiment was repeated with doses of 100, 200, 300, 400, 500, and 600 kGy. After irradiation, the sample was removed from the bottle, washed with double-distilled water, dried, and used for further characterization. PC by itself was also irradiated at the same doses with no $AgNO_3$ solution.

Characterization of the Ag–PC Matrix

The diffusion of Ag in PC was estimated by an RBS technique with a 2-MeV ^4He beam (with a 0° incidence angle and 165° laboratory scattering angle), and the backscattered particles were detected with a surface barrier detector with a detector active area of $80\,mm^2$ and a crystal thickness of 350 μm. The surface plasmon resonance of Ag was studied with a UV–vis spectrophotometer (Jasco, V-670) with PC as a reference in the wavelength range 300–700 nm. X-ray diffractograms were recorded in the 2θ range (10–80°) with a Bruker AXS D8 Advance X-ray diffractometer with Cu Kα radiation at a wavelength of 1.5406 Å. The surface morphology and atomic percentage (*A*) was studied with SEM (JEOL JSM 6390LV) attached with EDS and TEM (model Technai G^2 U-thin 200 kV, LaB_6 filament). To carry out TEM, a very small amount of Ag–PC sample was dissolved in methylene chloride and sonicated for an hour. Then, it was drop cast onto a carbon-coated TEM grid and allowed to dry under ambient conditions, and the TEM images were recorded. FTIR spectroscopy was carried out for all of the samples in transmittance mode with a Jasco 1600 FTIR spectrophotometer in the wave-number range 400–4000 cm^{-1} with 100 scans at a resolution of 1 cm^{-1}.

Positron Annihilation Lifetime and DB Measurements

The free-volume study of the γ-irradiated PC and Ag–PC samples were studied with PAS. When a positron from a radioactive source such as ^{22}Na enters a solid material, it will lose energy by colliding with electrons and thermalize. A thermalized positron may annihilate with an electron from any material and emit two γ photons within 0.2 ns, or it can be trapped in defects and open-volume sites, in which case its lifetime will increase up to 0.5 ns. However, in polymers, a thermalized positron may form a bound state of positronium (Ps) with unique time properties. Ps may be formed in either of two spin states of the electron and positron. *para*-Positronium (*p*-Ps) with antiparallel spins and a mean annihilation lifetime of 0.125 ns with the emission of two γ photons and *o*-Ps with parallel spins annihilating in free space with three-photon emission and a mean lifetime of 142 ns. However, in polymer systems, the lifetime of *o*-Ps may be shortened to 1–5 ns through the picking off of an electron of opposite spin from the surrounding medium and the emission of two photons. Before annihilation, the neutral *o*-Ps particles were localized in regions of low electron density, such as free-volume holes or cavities of the polymer. The probability of a pickoff process is related to the electron density near the cavity of the inner surface and, hence, to its size such that longer *o*-Ps lifetimes correspond to larger free-volume holes.[16–25]

The lifetime measurements were performed at room temperature with a fast–fast coincidence system with BaF_2 scintillators coupled to XP2020Q photomultiplier tubes. The positron lifetime spectrometer had a time resolution of 220 ps. A 30 μCi ^{22}Na positron source, deposited on Kapton foil is sandwiched between two identical pieces of the sample (1 mm thick). As the samples were thin films, they were stacked to obtain a 1 mm thick sample to ensure the annihilation of all positrons within the samples. Each spectrum containing at least 10^6 counts was analyzed with the PAT fit program.[28]

The DB measurements used a high-purity germanium detector with 1.1 keV (full width at half-maximum) of the 662 keV γ line of ^{137}Cs radioactive source and a constant channel width of 0.169 keV/channel. The source–sample sandwich prepared for positron lifetime measurement was placed at a distance of 20 cm away from the detector. This distance was long enough to prevent any increase in the background due to 3-γ annihilation. Around 10^6–10^7 counts were collected under each Doppler-broadened 511 keV γ-ray spectrum. The DB spectra were analyzed with the SP-I computer program to evaluate the line-shape parameters *S* and *W*.

Antibacterial Properties of Ag–PC Samples

The antibacterial activity of the Ag–PC samples against the Gram-negative bacteria *E. coli* and the Gram-positive bacteria *S. aureus* was studied by the agar well diffusion method. The samples were dissolved in dichloromethane and used for antibacterial activity. The bacterial cultures of known inoculum size (0.2 mL, 10^5 cfu/mL) of the test microorganisms were spread onto nutrient agar plates. In aseptic conditions, a sterile borer was used to prepare wells 5 mm in diameter in the nutrient agar medium of each Petri dish. The sample with a 2 mg concentration was used in each well, and the plates were incubated further for 18–24 h at 37 °C. The antibacterial activity was evaluated by the measurement of the zone of inhibition.

RESULTS AND DISCUSSION

RBS Results

RBS was carried out to study the diffusion of AgNPs in PC. The depth profile of the incorporated Ag atoms was determined by a simple channel-by-channel method with the energy dependence of the α-particle stopping power calculated for a pristine polymer with the database from the stopping and range of ions in matter (SRIM) code taken into account.[29] The RBS spectrum for the pristine PC and Ag–PC sample prepared at 600 kGy are shown in Figure 1. As shown in Figure 1, curve 2 showed a peak edge around 1725, which corresponded to Ag. The appearance of this peak edge confirmed the diffusion of Ag in PC, and the depth of diffusion of Ag in PC was found to be 1.02 μm. In our previous study,[30] we diffused gold nanoparticles in PC, and the diffusion depth of the gold nanoparticles in PC was found to be 0.85 μm. However, in the case of Ag–PC, the diffusion depth of the AgNPs in PC was found to be 1.02 μm. Therefore, the polymer surface was protected more against

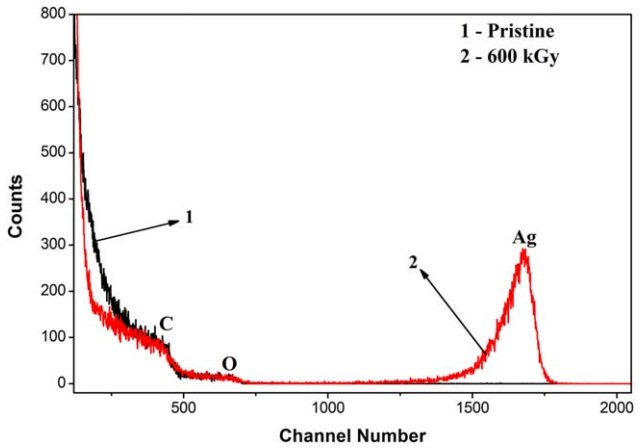

Figure 1. RBS spectrum for the (1) pristine PC and (2) Ag–PC matrix. [Color figure can be viewed in the online issue, which is available at wileyonlinelibrary.com.]

bacteria such as *E. coli* and *S. aureus* in the case of Ag–PC compared to that of gold–PC.

Optical and Structural Properties

The surface plasmon resonance of the AgNPs was studied with a UV–vis spectroscopic study, and the absorbance spectrum is shown in Figure 2. At a dose of 50 kGy, a small peak around 403 nm appeared that corresponded to Ag. The absorbance of this peak increased with the increase in the γ-ray dose, and also, it shifted toward a lower wavelength region; that is, it blue-shifted. A similar kind of variation was reported by Jelena *et al.*[11] The same was depicted in the mechanism section. This indicated that the particle size decreased with an increase in the γ-ray dose. The AgNPs present in PC were also confirmed by XRD, as shown in Figure 3. After irradiation, a peak appeared at 37.45° that corresponded to the (111) crystal planes of Ag with a face-centered cubic crystal structure.[5] The *d*-spacing corresponding to this angle was found to be 2.405 Å. The intensity of this peak increased with the increase in the γ-ray dose; this may have been because of the diffusion of more Ag in PC. Figure 4 shows the SEM images of the pristine PC and Ag–PC samples. We found from the SEM images also that the particle size of Ag decreased with increasing γ-ray dose. The *A* values of Ag in all of the samples were calculated with EDS, and they were found to increase with increasing γ-ray dose, as tabulated in Table I. Figure 5 shows the TEM images of the Ag–PC sample. The EDS spectra [Figure 5(f)] of TEM also showed the presence of Ag in the Ag–PC matrix (the copper peak in the EDS spectra was due to the copper grid used for TEM analysis). The TEM image showed [Figure 5(c)] the interplanar spacing to be 2.41 Å; this was in agreement with the XRD results and corresponded to the (111) crystal planes of Ag. The electron diffraction pattern of Ag [Figure 5(d)] showed that the AgNPs in PC were crystalline in nature. The average particle sizes of the AgNPs were found to be about 10 nm, as shown by the TEM analysis. All of these results confirmed the diffusion of the AgNPs in PC.

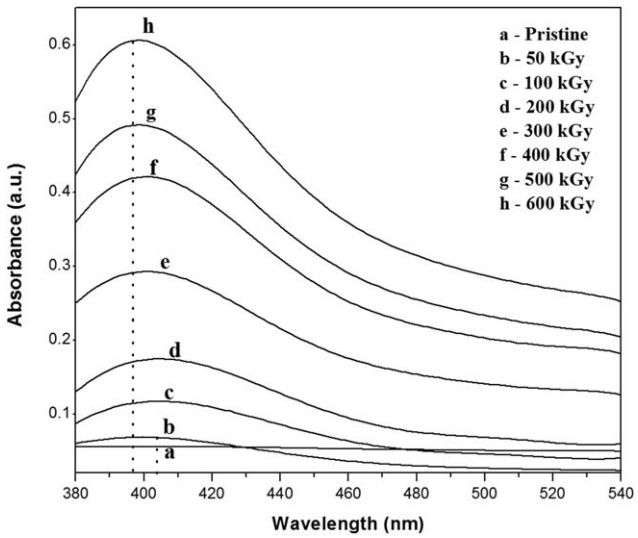

Figure 2. UV–vis spectrum for the pristine PC and Ag–PC matrix.

PAS

PAS was carried out to study the microstructural changes caused by γ-ray irradiation in the Ag–PC samples. To get clear information, we carried out PAS measurements for PC irradiated without the Ag solution at the same γ-ray doses. The typical PAS spectra for the pristine PC, γ-ray-irradiated PC (600 kGy), and Ag–PC (600 kGy) samples are shown in Figure 6(a). The obtained lifetime spectra were resolved into three-lifetime components, τ_1, τ_2, and τ_3, with the PAS fit program with variances χ^2 of fits of approximately 1 and with the respective intensities I_1, I_2, and I_3. The shortest lifetime, τ_1, with an intensity of I_1, was attributed to the annihilation of *p*-Ps and free positrons. The lifetime component, τ_2, with an intensity of I_2, was the contribution due to the positrons trapped at the defects present in the crystalline regions or trapped at the crystalline–amorphous interface regions. The longest lived component, τ_3, with an intensity of I_3, was due to the pickoff annihilation of *o*-Ps from the free-volume sites present mainly in the amorphous regions of the polymer matrix.[31] The long-life component (τ_3) of *o*-Ps responded very sensitively to the size and distribution of

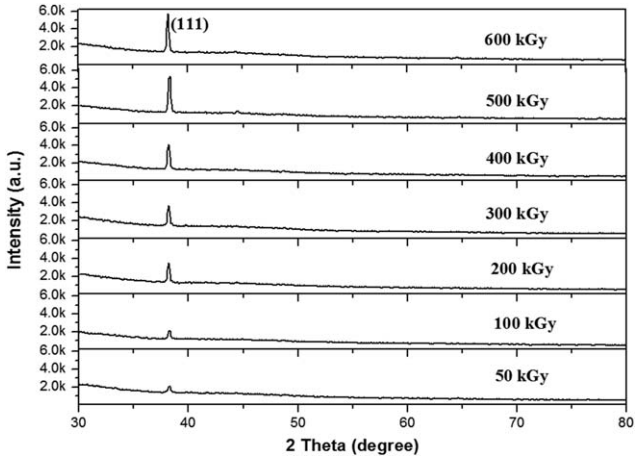

Figure 3. XRD of the Ag–PC matrix.

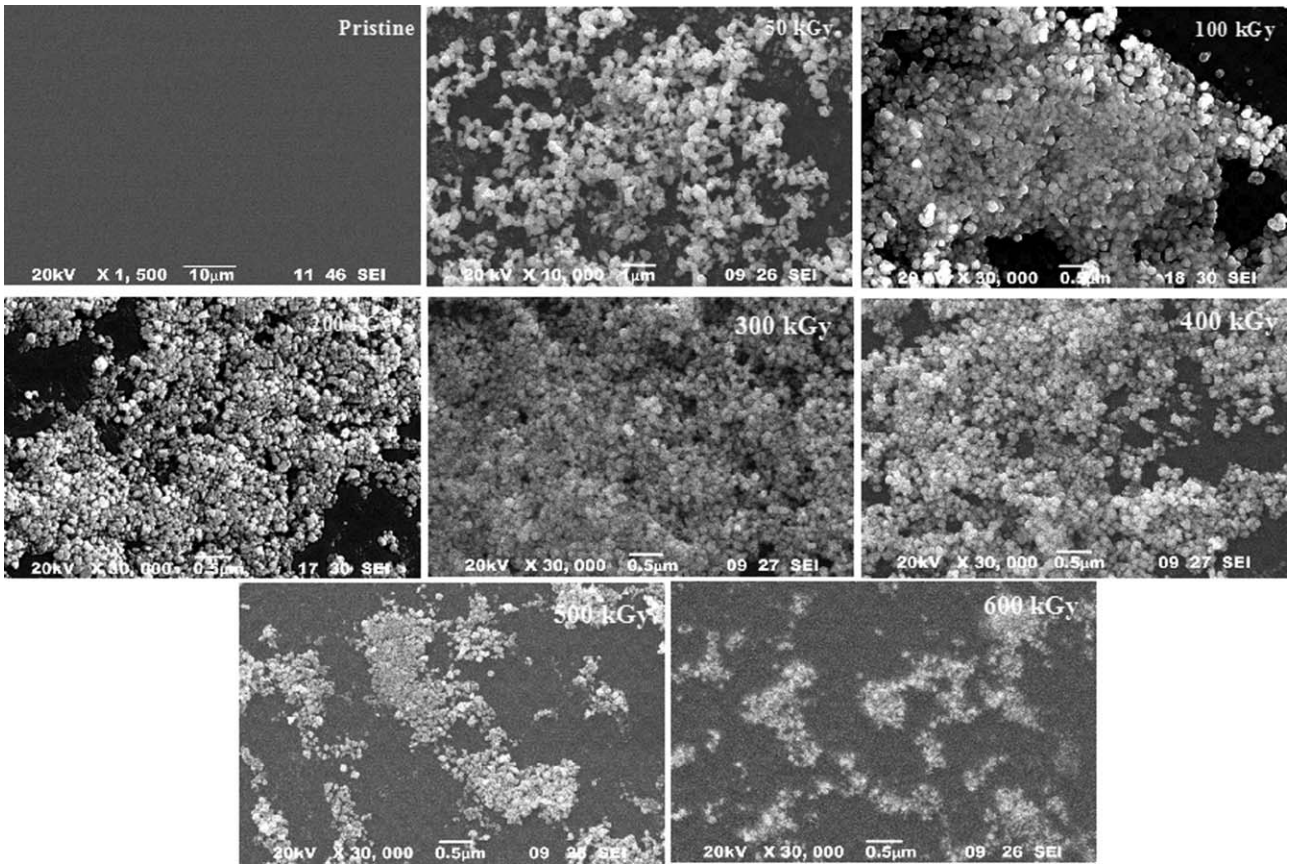

Figure 4. SEM images of the pristine PC and Ag–PC samples.

the free volumes, as Ps atoms were preferentially trapped in holes of atomic dimensions.

In this study, we used a relation connecting the *o*-Ps lifetime (τ_3) and free-volume hole radius (R) given by the following equation[32]:

$$\frac{1}{\lambda_3} = \tau_3 = 0.5\left[1 - \frac{R}{R+\Delta R} + \frac{1}{2\pi}\sin\left(\frac{2\pi R}{R+\Delta R}\right)\right]^{-1} ns \qquad (10)$$

where ΔR is a fitting parameter. The best fitted value of ΔR for all of the known data was 1.656 Å.[32] The average free-volume hole size (V_f) was then evaluated as $V_f = (4/3)\pi R^3$ and F_V, or the free-volume content, was given by

$$Fv = Cl_3 V_f \qquad (11)$$

where C is 0.0018 $Å^{-3}$.[22] The obtained values of τ_3, I_3, and V_f were tabulated for γ-ray-irradiated PC without and with Ag solution in Tables II and III, respectively.

The typical energy distribution curve of the Ag–PC sample (600 kGy) is shown in Figure 6(b). The ratio of the area of the central part of the DB spectrum (low momentum) to the total area under the DB spectrum gives *S*. *W* is taken in the high-momentum regions far from the center. It is the ratio of the area under the wings in a fixed window divided by the total area.[24,33–35] The momentum conservation in the annihilation process gives rise to a Doppler shift in the energies of individual γ rays. For positrons localized in open-volume defects, the fraction of valence electrons taking part in the annihilation process increases compared to that of core electrons, and because the momentum of valence electrons is significantly lower, the momentum distribution of annihilating electrons shifts to smaller values. This means a reduced Doppler shift (which leads to a smaller broadening of the annihilation peak, i.e., an increase in *S*) and provides the basis for defect studies. *S* and *W* are sensitive to the type and concentration of defects. *W* is more sensitive to the chemical environment than *S*, as core electrons have a higher momentum, and thus contributes mainly to the high-momentum regions of the spectra.[33–35]

The diffusion of AgNPs has a direct influence on the free volume of a polymer, and the diffusion of the dopant in such systems is controlled by the free volume and its content. Hence, the *o*-Ps τ_3 and I_3 are the most appropriate lifetime parameters for understanding the free-volume modifications because of the diffusion of AgNPs into PC. As shown in Table II and Figure 6, we observed that values of τ_3, I_3, and F_V for γ-ray-irradiated PC decreased with increasing dose, and at the highest dose, that is, at 600 kGy, a decrease in τ_3 was about 4.69%. The decreases in I_3 and F_V were associated with a decrease in the concentration of free-volume holes,[36] as a consequence of crosslinking process in the polymer matrix.[37] They could have been due to the formation of free radicals and the crosslinking of these free radicals with residual polymer.[20] Furthermore, the decrease in τ_3 could have been due to the chemical reaction of these free radicals with Ps.[38] In the crosslinked state, the polymer chains were

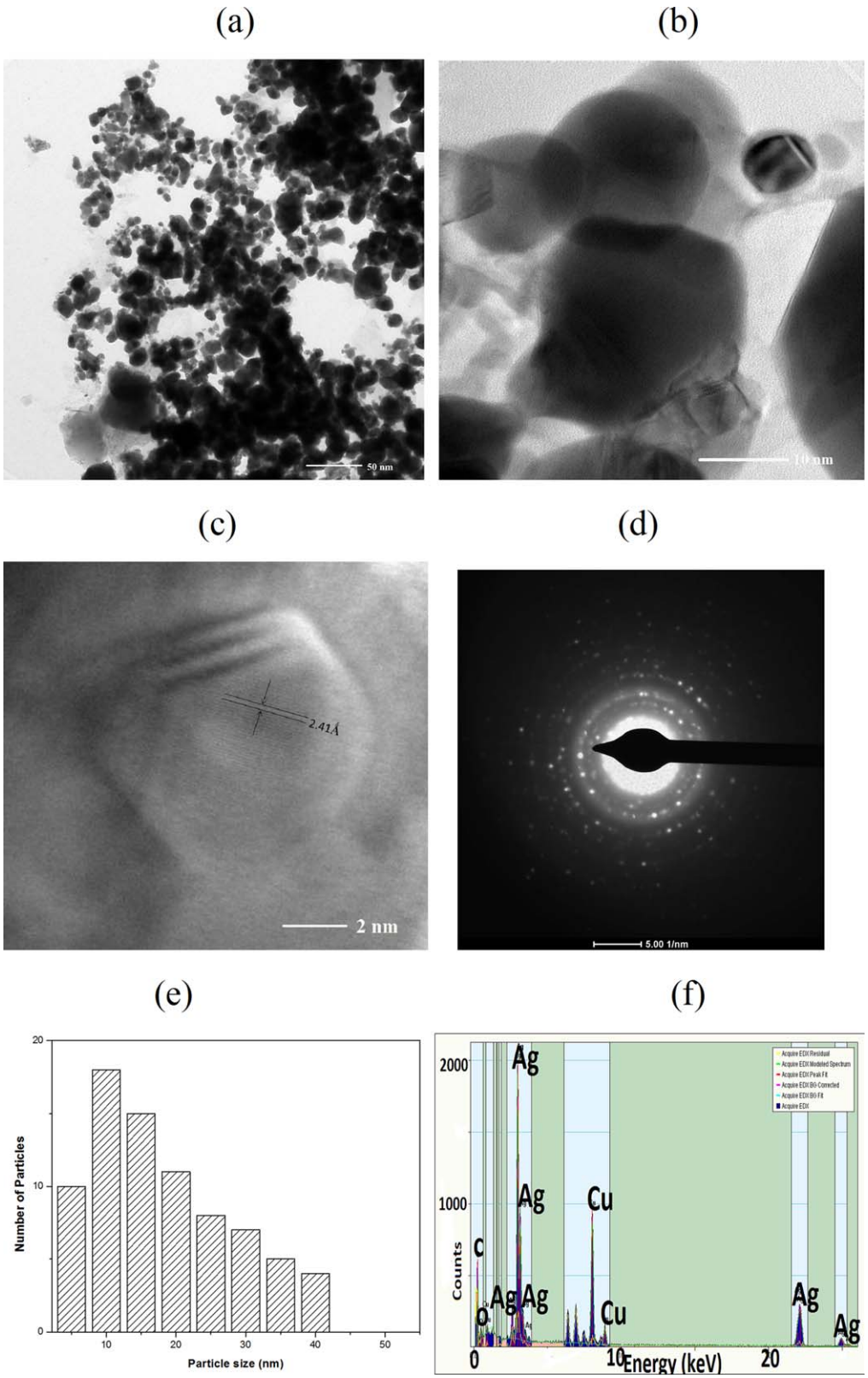

Figure 5. (a–c) TEM images of the Ag–PC matrix prepared at 600 kGy, (d) corresponding electron diffraction pattern, (e) particle size distribution, and (f) EDS. [Color figure can be viewed in the online issue, which is available at wileyonlinelibrary.com.]

Table I. *A* Values and Antibacterial Properties of the Ag–PC Matrix

Dose (kGy)	*A* (%)	Zone of inhibition (mm)	
		S. aureus	*E. coli*
50	0.02	1.3 ± 0.37	1.1 ± 0.10
100	0.26	1.6 ± 0.38	1.1 ± 0.46
200	0.31	1.8 ± 0.46	1.3 ± 0.22
300	0.49	2.1 ± 0.12	1.6 ± 0.20
400	—	2.3 ± 0.58	1.8 ± 0.31
500	0.95	2.8 ± 0.74	2.2 ± 0.36
600	1.28	3.2 ± 0.48	2.4 ± 0.15
Control (tetracycline)	—	12 ± 1.06	11 ± 0.35

expected to have closer packing; this would result in decreased sizes of the free-volume holes. This was evident from the decrease in the τ_3 values.

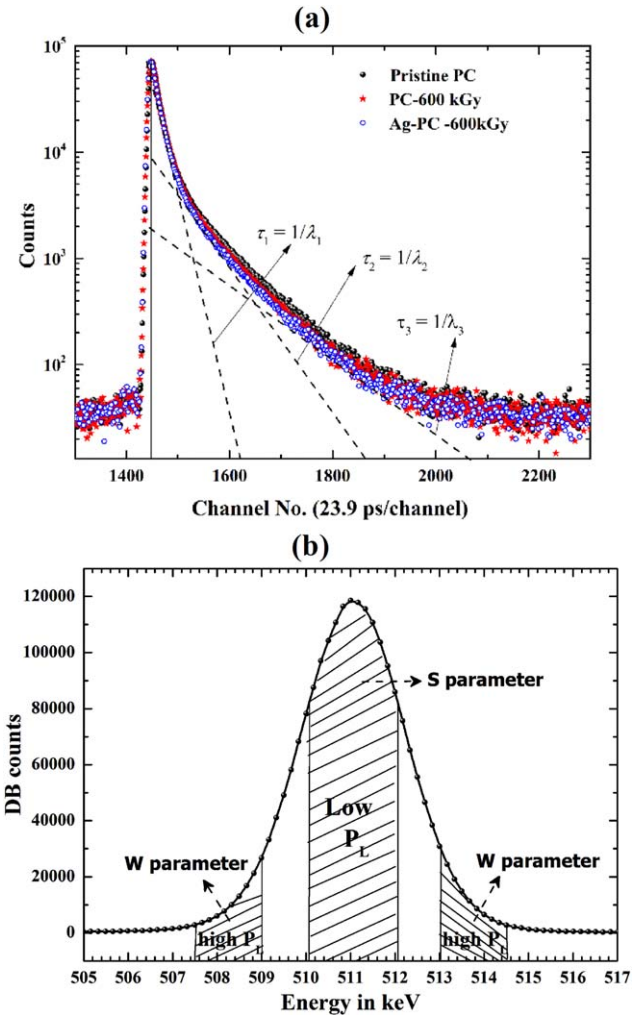

Figure 6. (a) Typical PAS spectrum for the pristine PC, γ-ray-irradiated PC (600 kGy), and Ag–PC sample (600 kGy). (b) Typical DB energy distribution curve of the Ag–PC matrix (600 kGy). P_L is the momentum. [Color figure can be viewed in the online issue, which is available at wileyonlinelibrary.com.]

Table II. PAS Results for the γ-Irradiated PC Samples

Dose (kGy)	$\tau_3 \pm 0.0089$ (ns)	$I_3 \pm 0.23$ (%)	$V_f \pm 0.8$ (Å^3)	F_V (%)
0	2.128	32.14	109.8	6.35
200	2.04	29.66	101.31	5.41
400	2.027	28.75	100.16	5.18
600	2.028	27.87	100.26	5.03

Similar to the γ-ray-irradiation of pristine PC, when the PC samples were irradiated in the Ag solution, the τ_3, I_3 (Table III), and F_V (Figure 7) values decreased gradually, and at 600 kGy, τ_3 decreased by 4.22%. The decrease in the values of τ_3, I_3, and F_V for this set of samples was attributed to the following:

1. The crosslinking of the polymer chains, which resulted in the close packing of polymer chains and, thereby, decreased the average free-volume size and number density of free-volume sites.
2. The diffusion of AgNPs into the free-volume holes.

Figure 8 shows the changes in *S* and *W* for the Ag-doped PC, as calculated from the DB spectrum. As shown in the figure, *S* decreased and *W* increased with increasing dose. This result was consistent with the RBS and XRD results, which show an increase in the diffusion of Ag particles into the polymer matrix as the irradiation dose increased. Furthermore, the electron diffraction pattern of Ag [see Figure 5(d)] showed that the AgNPs in PC were crystalline in nature. As the diffusion of Ag particles into the PC matrix increased, the overall crystalline region of the sample increased. Thus, with an increase in the dosage, the crystallinity of the sample increased; this was supported by the decrease in I_3 values.[23] This interpretation was in agreement with the PAS results given in Tables II and III.

The shape of the DB spectrum was determined by the momentum distribution of electrons with which the positron interacted, that is, valence or core, and the type of atom donating the electron. When the annihilation occurred in a large open-volume site, such as a defect in a crystalline material or free volume in an amorphous material (polymer), the fraction of low-momentum conductions and valence electrons (represented by *S*) participating in the process increases relative to the fraction of high-momentum core electrons (represented by *W*). Thus, a defect-rich/higher free-volume material will have a narrower electron momentum distribution than would a defect-free material. In this study of γ-ray-irradiated Ag–PC samples, as the

Table III. PAS Results for the Ag–PC Samples

Dose (kGy)	$\tau_3 \pm 0.0089$ (ns)	$I_3 \pm 0.23$ (%)	$V_f \pm 0.8$ (Å^3)	F_V (%)
0	2.128	32.14	109.8	6.35
200	2.069	30.71	104.17	5.76
400	2.025	29.55	99.95	5.32
600	2.038	28.31	101.21	5.16

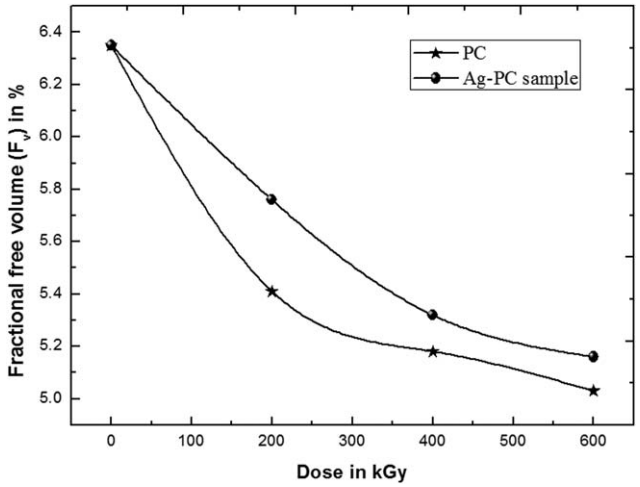

Figure 7. Variation of F_V with the γ-ray dose.

dosage increased, the free-volume size decreased, and the observed increase in *W* and the reduction in *S* were in complete agreement.

Thermal Properties

The thermal behavior of the pristine PC, γ-ray-irradiated PC (at 600 kGy), and Ag–PC sample (at 600 kGy) was studied with TGA and thermograms, as shown in Figure 9. All of the curves showed a stable zone up to 350 °C, and at high temperatures, Ag–PC showed little weight loss in comparison with the γ-ray-irradiated pristine PC samples. The γ-ray-irradiated PC sample showed a stable zone up to 385 °C, after which a slight weight loss up to 410 °C occurred, and then, a sudden decrease in the weight loss up to 520 °C occurred (fast decomposition zone). In this region, almost 80% of the sample was decomposed. The pristine PC showed a fast decomposition zone in the temperature range 440–540 °C, whereas the Ag–PC sample showed a fast decomposition zone in the temperature range 460–580 °C. The thermal decomposition temperature of the pristine PC was found to be 455 °C, whereas in the case of γ-ray-irradiated PC, it decreased to 440 °C, and in the case of the Ag–PC sample, it increased to 468 °C. This increase in the thermal decomposition temperature was due to the diffusion of AgNPs in PC, and the

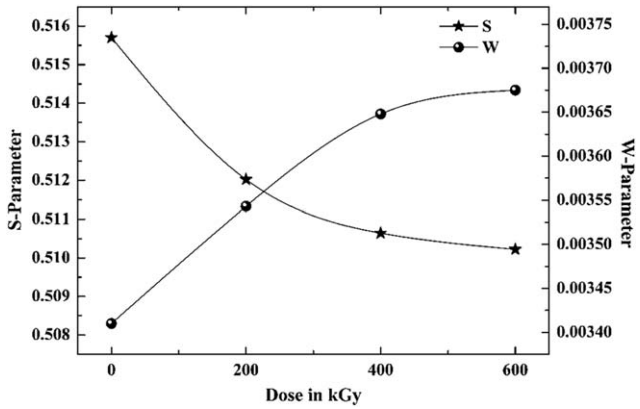

Figure 8. Plot of *S* and *W* as a function of the γ-ray dose for the Ag-doped PC.

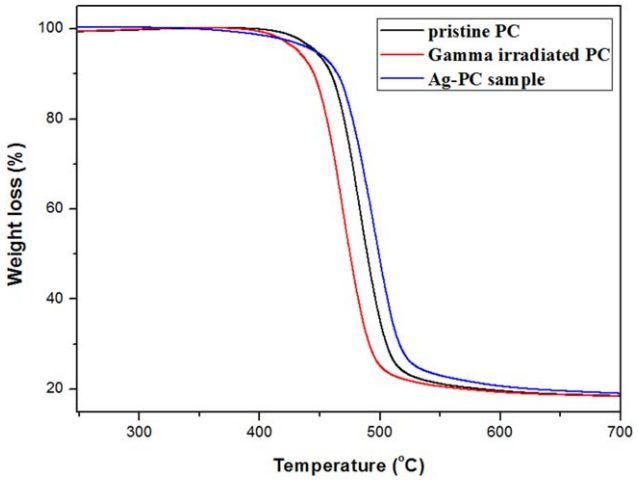

Figure 9. TGA curves for the pristine PC, γ-ray-irradiated PC, and Ag–PC samples at a dose of 600 kGy. [Color figure can be viewed in the online issue, which is available at wileyonlinelibrary.com.]

carboxyl groups in PC were expected to be the binding sites of the AgNPs. This may possibly have protected the polymer from thermal degradation; this was in agreement with the literature results.[9]

FTIR Spectroscopy

To understand the interaction between the AgNPs and PC matrix, FTIR spectroscopy of the pristine PC and Ag–PC samples were carried out, and they are shown in Figure 10. As no visible changes took place for the samples irradiated at 50 and 100 kGy, the FTIR spectra for these doses were not plotted. As shown in Figure 10, all of the curves exhibited the characteristic signature of the —CH_2—, benzene ring, and asymmetric vibrations of CH_3 at 1014, 1505, and 2968 cm^{-1}, respectively. The peaks present between the wave numbers 1150 and 1220 cm^{-1} were due to C—O—C vibrations.[38,39] It was clear that there was a change/decrease in the intensities of the band at 1014 cm^{-1} and bands between 1150 and 1220 cm^{-1}. This indicated the scissioning of the corresponding bonds after γ-ray irradiation. There must have been simultaneous crosslinking of polymer chains during irradiation, and this was confirmed by the new band that appeared prominently at 2884 cm^{-1} for samples irradiated at higher doses. This new bond was responsible for the asymmetric vibrations of CH_3.[39] A peak at 1558 cm^{-1} was assigned to the stretching band of C—O and shifted from 1558 to 1590 cm^{-1}. This shift identified that the oxygen lone pair in —C—O— participated in the interaction and was the main interaction between the surface of the AgNPs and PC chains; this confirmed the coordination between the Ag and oxygen atoms.[40]

Antibacterial Properties

The photographs (on a dark background) of the zone of inhibition of the pure PC, Gram-positive bacteria (*S. aureus*), and Gram-negative bacteria (*E. coli*) are shown in Figure 11. There were no antibacterial patterns in the pristine PC, but the Ag–PC sample showed a zone of inhibition pattern (some white patches) for both kinds of bacteria. The zones of inhibition by the prepared Ag–PC sample are given in Table I, and they showed moderate antibacterial activity against both Gram-

negative and Gram-positive bacteria. The zone of inhibition by the Ag–PC sample may have been due to the following two reasons:

1. AgNPs produced reactive oxygen species in the vicinity of the bacterial cell membrane, and this led to the cell permeability and, hence, cell death.[41,42]
2. The metallic nanostructures may have released metal ions slowly from the surface, and this might have interacted with the DNA and cellular enzymes. This was done by the coordination of electron-donating groups of microbes.[43,44]

The damage to the cell membrane resulted in the disruption of respiratory chain reactions. In such a way, metal ion–DNA interaction inhibited bacterial cells and finally killed the cells.[45] In addition, as shown in Table I, the zone of inhibition was greater in the case of Gram-negative bacteria compared to that of Gram-positive bacteria; this may have been due to the difference in their cell wall structure. The cell wall of the Gram-positive bacteria consisted of a thick layer of peptidoglycan (linear polysaccharide chains crosslinked by short peptides) and thus formed a more rigid structure; this led to difficulty for the AgNPs to penetrate inside the cell, but the cell walls of the Gram-positive bacteria possessed a thinner layer of peptidoglycan.[46]

CONCLUSIONS

The Ag–PC samples were prepared by an easy and cost-effective approach. The RBS results show the diffusion of Ag in PC down to a depth of 1.02 μm. The surface plasmon resonance of the AgNPs decreased with increasing dose; this indicated the decrease in the particle size of Ag, which was also corroborated by the SEM results. The XRD results reveal that the diffused AgNPs had an FCC structure, and this was supported by the TEM results. The effects of γ-radiation with various dosages on the PC and Ag–PC samples were studied through PAS. The observed reduction in lifetime parameters was due to the crosslinking of chains and the diffusion of AgNPs into the amorphous region of the polymer matrix. These results were further supported by *S* and *W*. The immobilization of AgNPs in PC increased the thermal decomposition temperature of the Ag–PC sample. The zone of inhibition of both the Gram-positive and Gram-negative bacteria increased with increasing dose for the prepared sample because of the decrease in the Ag particle size with γ-ray dose. The prepared Ag–PC matrix may find uses in the food industry and medical applications.

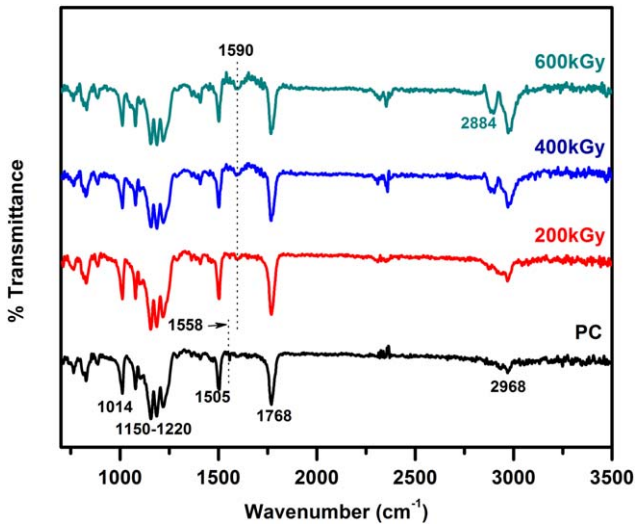

Figure 10. FTIR spectra of the PC and Ag–PC samples. [Color figure can be viewed in the online issue, which is available at wileyonlinelibrary.com.]

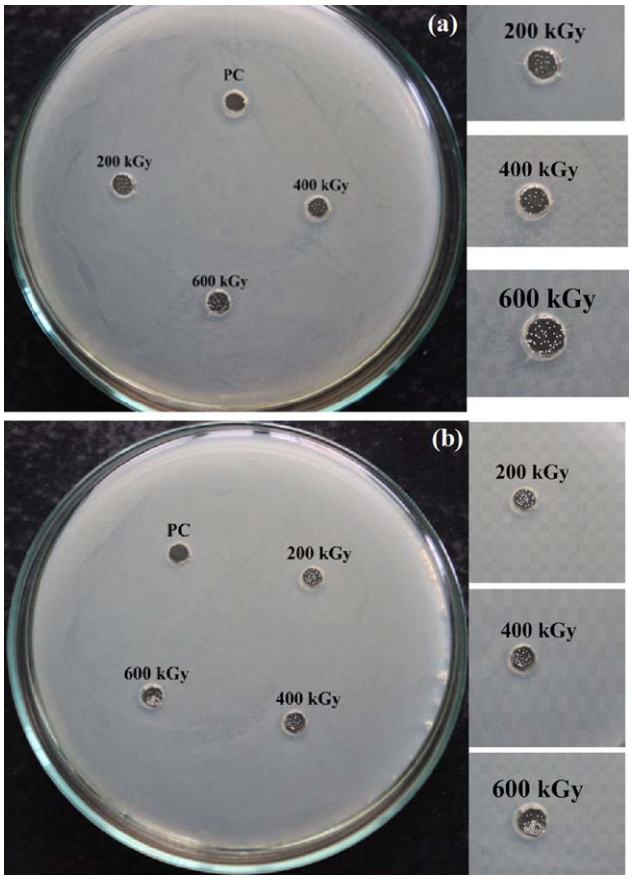

Figure 11. Antibacterial effects of the Ag–PC samples on (a) *E. coli* and (b) *S. aureus* along with pristine PC. [Color figure can be viewed in the online issue, which is available at wileyonlinelibrary.com.]

ACKNOWLEDGMENTS

Two of the authors (A.V.D. and K.H.) thank the University Grants Commission (Government of India) for its support (in the form of a University Grants Commission–Basic Scientific Research grant and a D. S. Kothari Postdoctoral Fellowship, respectively). The authors acknowledge Lochab, Mr. Birender, and Mr. Sunil Ojha (Inter-University Accelerator Centre, New Delhi, India) for providing the γ-radiation and RBS facility. This research was also supported by the University of Western Australia and the Australian Research Council.

REFERENCES

1. Anil, D.; Conn, B. E.; Guo, J.; Yoon, B.; Barnett, R. N.; Monahan, B. M.; Kirschbaum, K.; Griffith, W. P.; Whetten, R. L.; Landman, U.; Bigioni, T. P. *Nat. Lett.* **2013**, *501*, 399.

2. Tran, Q. H.; Nguyen, V. Q.; Le, A. T. *Adv. Nat. Sci. Nanosci. Nanotechnol.* **2013**, *4*, 033001.
3. Belloni, J.; Mostafavi, M. Radiation Chemistry: Present Status and Future Trends; Elsevier: Amsterdam, **2001**.
4. Mahapatra, S. K.; Bogle, K. A.; Dhole, S. D.; Bhoraskar, V. N. *Nanotechnology* **2007**, *18*, 135602.
5. Bogle, K. A.; Dhole, S. D.; Bhoraskar, V. N. *Nanotechnology* **2006**, *17*, 3204.
6. Pattabi, M.; Pattabi, R. M.; Sanjeev, G. *J. Mater. Sci. Mater. Electron.* **2009**, *20*, 1233.
7. Misra, N.; Biswal, J.; Dhamgaye, V. P.; Lodha, G. S.; Sabharwal, S. *Adv. Mater. Lett.* **2013**, *4*, 458.
8. Vacik, J.; Hnatowicz, V.; Dhole, S. D.; Mathakari, N. L.; Dahiwale, S. S.; Bogale, K. B.; Bhoraskar, V. N. *Radiat. Phys. Chem.* **2014**, *98*, 92.
9. Lu, Z.; Meng, M.; Jiang, Y.; Xie, J. *Colloids Surf. A* **2014**, *447*, 1.
10. Eisa, W. H.; Abdel-Moneam, Y. K.; Shaaban, Y.; Abdel-Fattah, A. A.; Zeid, A. M. A. *Mater. Chem. Phys.* **2011**, *128*, 109.
11. Jelena, K.; Jelena, S.; Aleksandra, R.; Aleksandra, P. G.; Duric, M.; Zorica, K. P.; Popovic, S. *J. Appl. Polym. Sci.* **2014**, *131*, 40321.
12. Krkljes, A. N.; Marinovic-Cincovic, M. T.; Kacarevic-Popovic, Z. M.; Nedeljkovic, J. M. *Eur. Polym. J.* **2007**, *43*, 2171.
13. Yu, D.; Sun, X.; Bian, J.; Tong, Z.; Qian, Y. *Phys. E* **2004**, *23*, 50.
14. Jovanovic, Z.; Radosavljevic, A.; Siljegovic, M.; Bibic, N.; Vesna, M. S.; Zorica, K. P. *Radiat. Phys. Chem.* **2012**, *81*, 1720.
15. Li, T.; Park, H. G.; Choi, S. H. *Mater. Chem. Phys.* **2007**, *105*, 325.
16. Mukherjee, M.; Chakravorty, D.; Nambissan, P. M. G. *Phys. Rev. B* **1998**, *57*, 848.
17. Zaleski, R.; Kierys, A.; Grochowicz, M.; Dziadosz, M.; Goworek, J. J. *Colloid Interface Sci.* **2011**, *358*, 268.
18. Awad, S.; Chen, H.; Chen, G.; Gu, X.; Lee, J. L.; Abdel-Hady, E. E.; Jean, Y. C. *Macromolecules* **2011**, *44*, 29.
19. Narkis, M.; Sibony-Chaout, S.; Siegmann, A.; Shkolnik, S.; Bell, J. P. *Polymer* **1985**, *26*, 50.
20. Hama, Y.; Shinohara, K. *J. Polym. Sci. Part A-1: Polym. Chem.* **1970**, *8*, 651.
21. Singh, P.; Kumar, R.; Singh, R.; Roychowdhury, A.; Das, D. *Appl. Surf. Sci.* **2015**, *328*, 482.
22. Jean, Y. C. *Microchem. J.* **1990**, *42*, 72.
23. Nakanishi, H.; Jean, Y. C. *Macromolecules* **1991**, *24*, 6618.
24. Ramya, P.; Guagliardo, P.; Pasang, T.; Ranganathaiah, C.; Samarin, S.; Williams, J. F. *Phys. Rev. E* **2013**, *87*, 052602.
25. Fan, Y. M.; Zhang, X.; Ye, B.; Zhou, X.; Weng, H.; Du, J.; Han, R.; Jao, S.; Zhang, Z. *Chin. J. Polym. Sci.* **2002**, *20*, 243.
26. Zhou, Y.; Yu, S. H.; Wang, C. Y.; Li, X. G.; Zhu, Y. R.; Chen, Z. Y. *Adv. Mater.* **1999**, *11*, 850.
27. Naghavi, K.; Saion, E.; Rezaee, K.; Yunus, W. M. M. *Radiat. Phys. Chem.* **2010**, *79*, 1203.
28. Olsen, J. V.; Kirkegaard, P.; Pedersen, N. J.; Eldrup, M. M. *Phys. Status Solidi C* **2007**, *4*, 4004.
29. Ziegler, J. F.; Ziegler, M. D.; Biersack, J. P. *Nucl. Instrum. Methods Phys. Res. B* **2010**, *268*, 1818.
30. Hareesh, K.; Deore, A. V.; Dahiwale, S. S.; Sanjeev, G.; Kanjilal, D.; Ojha, S.; Dhole, N. A.; Kodam, K. M.; Bhoraskar, V. N.; Dhole, S. D. *Radiat. Phys. Chem.* **2015**, *112*, 97.
31. Nakanishi, H.; Jean, Y. C.; Smith, E. G.; Sandreczki, T. C. *J. Polym. Sci. Part B: Polym. Phys.* **1989**, *27*, 1419.
32. Proceedings of the International Symposium on Positron Annihilation Studies in Fluids; Nakanishi, H., Wang, S. J., Jean, Y. C., Sharma, S. C., Eds.; World Scientific: Singapore, **1988**.
33. Nagai, Y.; Nonaka, T.; Hasegawa, M.; Kobayashi, Y.; Wang, C. L.; Zheng, W.; Zhang, C. *Phys. Rev. B* **1999**, *60*, 11863.
34. Krause-Rehberg, R.; Leipner, H. S. Positron Annihilation in Semiconductors; Springer: Berlin, **1999**; vol. *127*.
35. Zhang, R.; Robles, J.; Kang, J. *Macromolecules* **2012**, *45*, 2434.
36. Wang, B.; Zhang, M.; Zhang, J. M.; He, C. Q.; Dai, Y. Q.; Wang, S. J.; Ma, D. Z. *Phys. Lett. A* **1999**, *262*, 195.
37. Ramani, R.; Shariff, G.; Thimmegowda, M. C.; Sathyanarayana, P. M.; Ashalatha, M. B.; Balraj, A.; Ranganathaiah, C. *J. Mater. Sci.* **2003**, *38*, 1431.
38. Buttafava, A.; Consolati, G.; Landro, L. D.; Mariani, M. *Polymer* **2002**, *43*, 7477.
39. Sinha, D.; Sahoo, K. L.; Sinha, U. B.; Swu, T.; Chemseddine, A.; Fink, D. *Radiat. Effects Defects Solids* **2004**, *159*, 587.
40. Ye, S.; Chen, S.; Fang, L.; Lu, Y. *J. Mater. Chem.* **2010**, *20*, 3827.
41. Ivan, S.; Branka, S. S. *J. Colloid Interface Sci.* **2004**, *275*, 177.
42. Maness, P. C.; Smolinski, S.; Blake, D. M.; Huang, Z.; Wolfrum, E. J.; Jacoby, W. A. *Appl. Environ. Microbiol.* **1999**, *65*, 4094.
43. Smetana, A. B.; Klabunde, K. J.; Marchin, G. R.; Sorensen, C. M. *Langmuir* **2008**, *24*, 7457.
44. Feng, Q. L.; Wu, J.; Chen, G. Q.; Cui, F. Z.; Kim, T. N.; Kim, J. O. *J. Biomed. Mater. Res.* **2000**, *52*, 662.
45. Singh, S.; Patel, P.; Jaiswal, S.; Prabhune, A. A.; Ramana, C. V.; Prasad, B. L. V. *New J. Chem.* **2009**, *33*, 646.
46. Kaviya, S.; Santhanalakshmi, J.; Viswanathan, B.; Muthumary, J.; Srinivasan, K. *Spectrochim. Acta Part A* **2011**, *79*, 594.